Failure Analysis and Recovery of a 50-mm Highly Elastic Intermetallic NiTi Ball Bearing for an ISS Application

Christopher DellaCorte*, S. Adam Howard* and Lewis E. Moore III†

Abstract

Ball bearings used inside the ISS Distillation Assembly centrifuge require superior corrosion and shock resistance to withstand acidic wastewater exposure and heavy spacecraft launch related loads. These requirements challenge conventional steel bearings and provide an ideal pathfinder application for 50-mm bore, deep-groove ball bearings made from the corrosion immune and highly elastic intermetallic material 60NiTi. During early ground testing in 2014 one 60NiTi bearing unexpectedly and catastrophically failed after operating for only 200 hr. A second bearing running on the same shaft was completely unaffected. An investigation into the root cause of the failure determined that an excessively tight press fit of the bearing outer race coupled with NiTi's relatively low elastic modulus were key contributing factors. The proposed failure mode was successfully replicated by experiment. To further corroborate the root cause theory, a successful bearing life test using improved installation practices (selective fitting) was conducted. The results show that NiTi bearings are suitable for space applications provided that care is taken to accommodate their unique material characteristics.

Introduction

Bearings, gears and other mechanical components can be made from a wide variety of materials depending upon application requirements that typically include load, temperature, environment and cost [1, 2]. Often, one overriding performance requirement dictates that a specific material be selected. In cases where multiple requirements preclude certain classes of materials, practical designs can become difficult.

For instance, if a bearing must operate at high temperature but also be lightweight neither plastic nor steel would suffice. In such cases, the designer might have to turn to higher cost ceramics. Alternatively, the application requirements could be altered through system design changes to accommodate a lower cost material. A common engineering solution for the aforementioned high temperature example is to employ active cooling which enables the use of low-density plastics or non-ferrous alloys. Such accommodations themselves add cost and complexity and in many aerospace applications are not practical.

Another example where conventional bearing materials fall short are applications that simultaneously require extreme corrosion resistance and tolerance to severe static loads (shock events). Taken separately, these attributes can be found in austenitic stainless steels or superalloys (corrosion resistance) and ceramics or high carbide tool steels (shock load resistance). Taken together, these attributes cannot be provided by existing bearing materials [3].

Over the last decade NASA has been working to develop a new class of bearing materials based upon Nickel-Titanium to address these and other unmet challenges encountered in aeronautics and space mechanism bearing applications [4-6]. As an example, 60NiTi (60 weight% Ni, 40 weight% Ti) is hard, highly corrosion resistant, non-magnetic, electrically conductive, wear resistant, readily machined in the annealed state and exhibits good tribological properties. 60NiTi is also superelastic exhibiting a moderate

* NASA Glenn Research Center, Cleveland, OH

† NASA Marshall Space Flight Center, Huntsville, AL

elastic modulus coupled with an ability to endure large strains elastically. The combination of excellent corrosion resistance and high dent resistance (arising from the high hardness, low modulus and superelasticity) distinguish 60NiTi from the tool steels and ceramics commonly used in bearings. Table I compares bearing relevant properties of 60NiTi to conventional materials.

Table I. Thermophysical and mechanical properties of 60NiTi and other bearing materials

Property	**60NiTi**	**440C**	**Si_3N_4**	**M-50**
Density	6.7 g/cc	7.7 g/cc	3.2 g/cc	8.0 g/cc
Hardness	56–62 Rc	58–62 Rc	1300–1500 Hv*	60–65Rc
Thermal Cond. W/m-°K	~9–14	24	33	~36
Thermal Expansion	~11.2×10^{-6}/°C	10×10^{-6}/°C	2.6×10^{-6}	~11×10^{-6}/°C
Magnetic	Non	Magnetic	Non	Magnetic
Corrosion Resistance	Acceptable (in acids)	Marginal	Acceptable	Poor
Tensile/Flexural Strength	~1000/1500 MPa	1900 MPa	600–1200 MPa (Bend Strength)	2500 MPa
Young's Modulus	~90–115 GPa	200 GPa	310 GPa	210 GPa
Poisson's Ratio	~0.34	0.30	0.27	0.30
Fracture Toughness	~20 MPa/√m	22 MPa/√m	5–7 MPa/√m	20–23 MPa/√m
Max. Use Temp	~400 °C	~400 °C	~1100 °C	~400 °C
Elect. Resistivity	~1.04×10^{-6} Ω-m	~0.60×10^{-6} Ω-m	Insulator	~0.18×10^{-6} Ω-m

*Vicker's hardness, Hv, is a scale used for ceramic materials with hardness values beyond HRC 75.

A NASA application requiring corrosion resistance and high load capacity is inside the International Space Station (ISS) Urine Processor Distillation Assembly [7]. The Urine Processor Distillation Assembly (DA) is a key component of the wastewater treatment system on the ISS. The DA functions as a rotating still that processes waste fluids into steam (gaseous water). Figure 1 shows a cross section of the Urine Processor [8]. It consists of a rotating drum made from titanium alloy supported on a pair of 50-mm ball bearings and is driven by a motor at a constant speed of 200 rpm. The wastewater is introduced into the drum through a feed tube. Through centrifugal action, the rotating motion of the drum forces the wastewater into contact with the drum walls. The drum walls are heated and this boils the wastewater, forming steam that is drawn from the evaporator drum, condensed and then further treated downstream into clean water. The 50-mm bore ball bearings that support the rotating drum are directly exposed to the acidic wastewater and the steam environment and have experienced corrosion problems when made from steel. The use of NiTi is intended to avoid the corrosion problems yet provide good load capacity and wear life.

In a previous test and development program, 60NiTi ball bearings were designed and fabricated for use in the DA centrifuge [9]. Corrosion tests were performed to confirm the chemical compatibility with the wastewater environment and static load experiments were done to show that the bearings would endure anticipated launch loads. As a proof of concept, short-term (~20 hr) bearing tests were run in a simulator test rig that duplicated the load, speed, temperature and moisture conditions found inside the DA, albeit without the low pH acidic fluid nature. These tests were successful and a flight bearing project was initiated.

During the ground test phase of the project, a pair of 60NiTi centrifuge bearings were installed in a fully operational DA and placed into a long-term test program intended to run for up to 2000 hr. After only 200 hr, nickel and titanium particles were observed in the process fluid filtration system. After 235 hr of run time audible bearing noise was emanating from the centrifuge and the test was halted. An inspection revealed catastrophic failure of the hub-side (left side in Figure 1) 60NiTi centrifuge bearing. The second bearing of the pair, which operated on the same shaft on the motor-side of the DA, remained in good condition and showed no signs of distress. In the following sections of this paper, the results of the hub-

side bearing failure investigation are presented along with the development of the likely root cause and failure recovery.

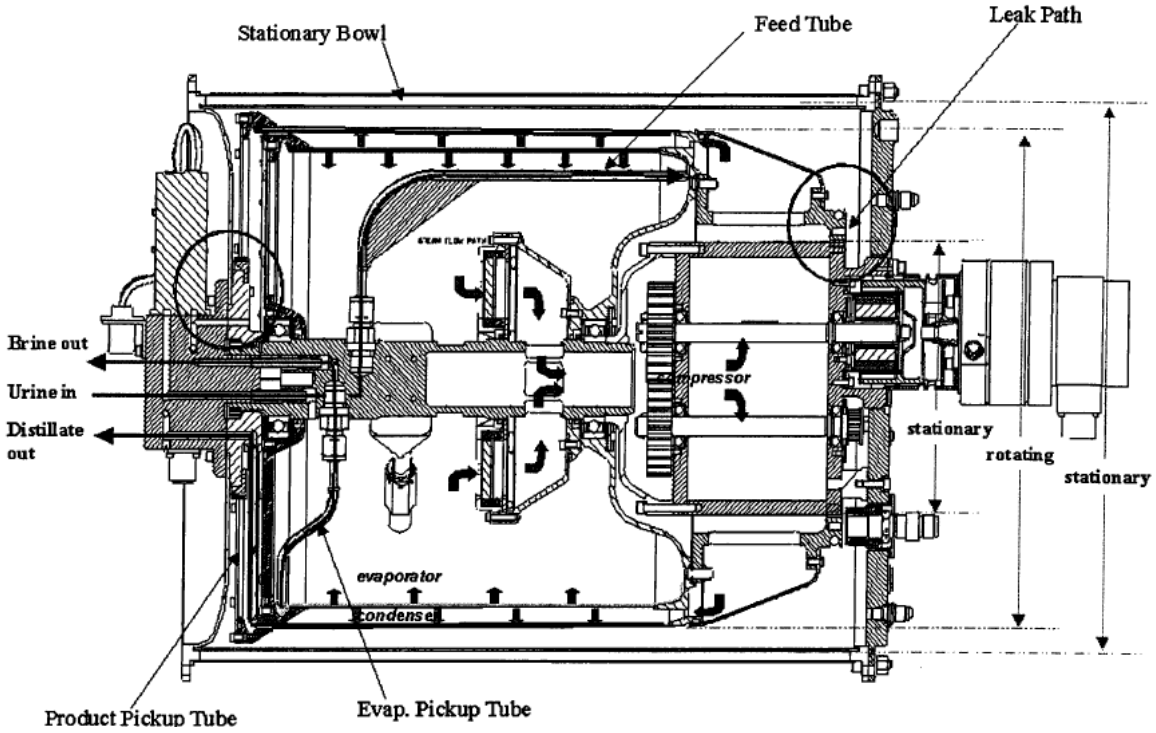

Figure 1. Representative ISS Distillation Assembly cross-section taken from reference 8

Bearing Design and Operating Conditions

Table II lists the nominal operating conditions and the bearing characteristics for the 50-mm bearings. The load on both bearings comes primarily from the preload wave spring. The outer races use an interference press fit into the drum end walls and the inner races slide over the shaft with a small clearance.

Table II. Representative Application Bearing Parameters and Operating Conditions

Parameter	Value or Condition
Outer Diameter, OD	~80 mm
Inner Diameter, ID	~50 mm
Width, W	~16 mm
Ball Size, D	~9 mm
Ball Material	Si_3N_4
Race Material	60NiTi
Cage	Snap fit, polymer
Lubricant	Lithium based grease
Ball-Race Stress Limit	~3.1 GPa
Ball-Race Mean Stress	~1 GPa
Axial Preload	~200 N
Radial Load (terrestrial)	~100 N/bearing
Speed	100-300 rpm
Environment	Warm, highly acidic aqueous solution
Ambient Pressure	Slight vacuum

The operating loads and speeds are low for a 50-mm bearing. In this application, the bearing size was largely dictated by the need to accommodate a large, stationary hollow shaft that houses electrical and fluid flow passageways into and out of the drum assembly. Other than potentially severe vibration loads (~3 g or higher) during a rocket launch, the operating conditions are characterized as mechanically benign and chemically aggressive. Since the 60NiTi alloy had previously been shown to be impervious to the acidic wastewater, the premature bearing failure was unexpected.

Hardware Observations and Other Forensic Evidence

The presence of nickel-titanium wear debris trapped by the DA filter screens indicated that bearing wear had occurred prior to failure. Following test termination, the hub-side end wall plate of the DA was removed making one face of the bearing visible. Figure 2 shows the view from the hub-side of the DA looking towards the motor-side.

Based upon this image alone, one plausible preliminary failure scenario is that the inner race fractured and caused more generalized damage and wear as the test continued. A close up image of the inner race fracture, shown in Figure 3, offers additional clues to the behavior of the 60NiTi.

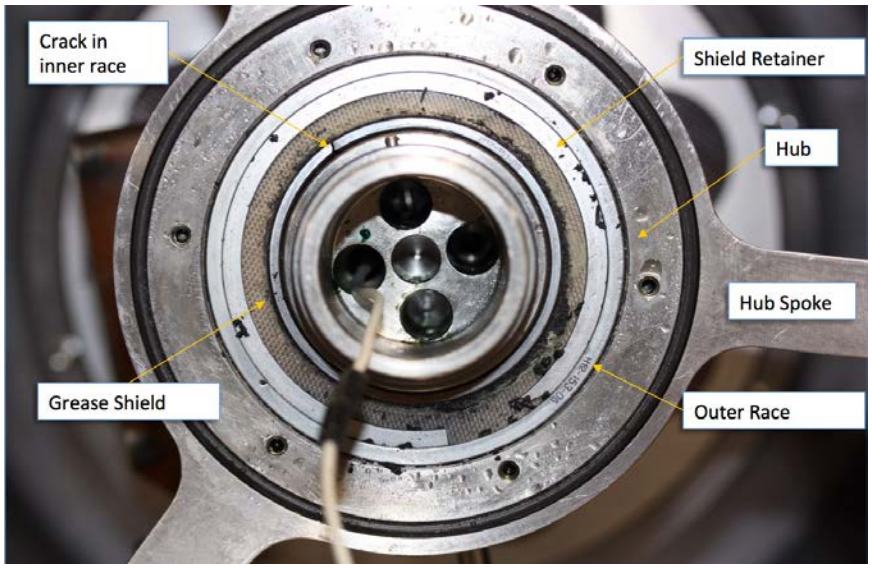

Figure 2. Hub-side view of failed ISS Distillation Assembly centrifuge bearing. Note cracked inner race and ejected wear debris

The inner race appears to have sprung radially outward from the DA shaft to the left side of the crack and a significant gap has opened between the faces of the crack. This behavior suggests that the inner ring had been under considerable residual stresses and these may have been a factor in the bearing failure.

Indeed, the bearing manufacturing process for 60NiTi includes a rapid water quench step following heat treatment at 1000 °C [9]. This rapid cooling results in the rise of residual thermal stresses. Unlike steels and other metals in which such residual stresses can be relieved by soaking the parts at elevated temperatures, NiTi has no mechanism for internal atomic level slip. The residual stresses that remain after the quenching step cannot be relieved through additional thermal treatments and these stresses may be a factor in undesirable effects like ring cracks [10, 11].

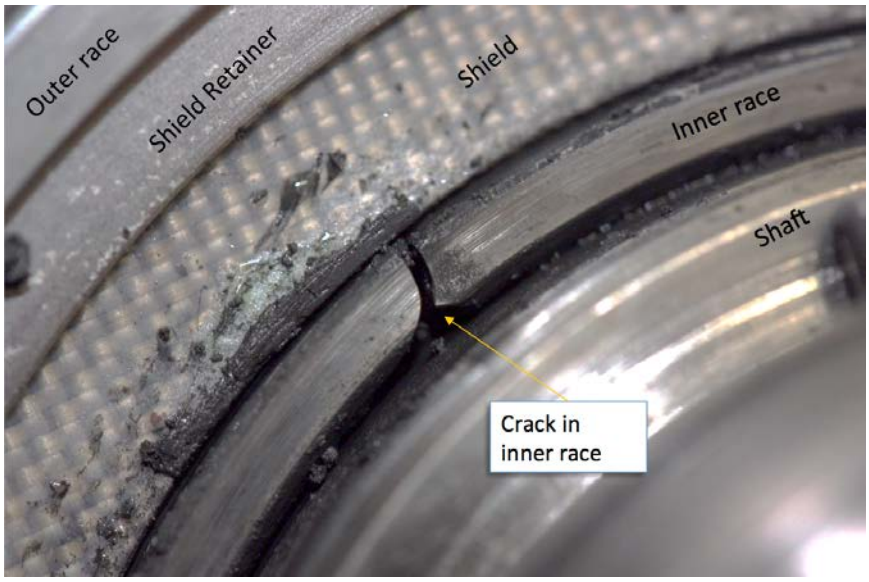

Figure 3. Close-up view of cracked inner race

A similar bearing ring crack was observed during prototype bearing development. A bearing had been successfully tested, removed from the test rig and inspected. The bearing was in as-new condition and was placed in storage. Several weeks later, the inner ring developed a crack similar to the one observed in the present case. Figure 4 shows that inner ring crack.

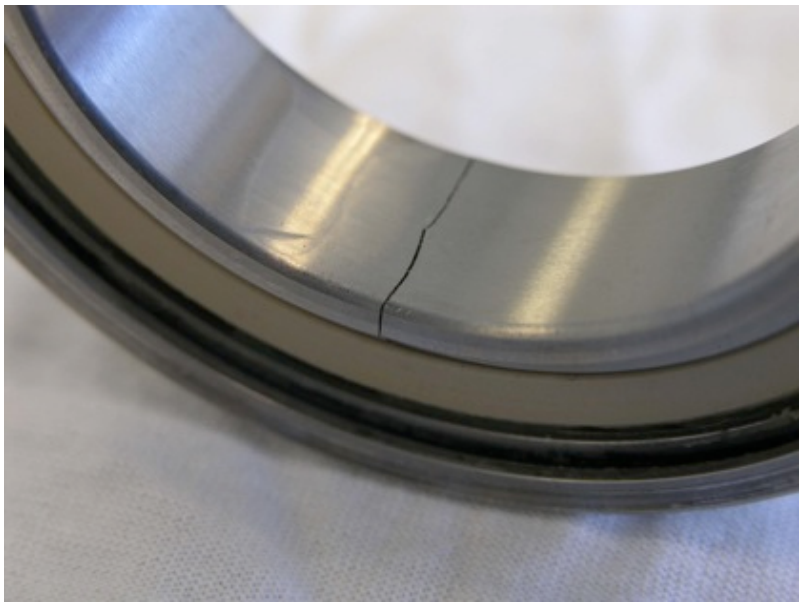

Figure 4. Photo of an early prototype bearing that developed an inner race crack during post-test storage

In this instance, forensic analyses showed that the early prototype 60NiTi material used in this bearing contained significant non-metallic inclusions and other internal flaws that could have triggered the crack. In addition, the bearing was damaged during final machining of the inside surface of the inner ring. Adjacent to the fracture location, a low spot and a deep gouge are observed. This damage was a

manufacturing flaw that resulted from the inner ring becoming loose in the machining fixture. Thus this post-test ring crack was attributed to the known material and machining flaws [11].

For the bearing failure that is the subject of the current paper, the material was known to be of the highest quality and absent of similar dimensional errors (low spots) or manufacturing flaws. To fully understand the present bearing failure more detailed information regarding the application and installation are needed.

The bearings were dimensionally characterized two times: once during manufacture by the bearing finisher and once immediately prior to installation by the NASA MSFC Tribology Lab. In general, both bearings were found to be within specification for all major diameters and widths, raceway curvatures and surface finishes. All of the construction materials (balls, cages, race material, etc.) were fully certified for quality. Visual inspection of the bearings revealed no observable flaws and both bearings turned smoothly. The only significant discrepancy between the bearing finisher's dimensions and those from the MSFC lab pertained to the bearings' outside diameter and roundness. The MSFC lab noted that the bearing outer race roundness values were affected by the installation of the grease shield retaining wires. These "C" shaped retaining wires are pre-compressed and then installed in a groove machined in the outer bearing race adjacent to the shield. The wires apply a small expansion load on the outer race causing it to become non-circular (slightly oval). This rather surprising observation is likely the result of the relatively low elastic modulus of the 60NiTi. In any case, the magnitude of the roundness variation was small (less than 0.0002 in or 5 µm) and deemed unlikely to affect the bearing operation once confined (pressed into) by the DA hub structure.

Unfortunately, the failed bearing could not be removed from the DA intact. Disassembly forces fractured the outer race into several pieces making forensic interpretation of the damage impossible. Further, since the DA was operated long after significant bearing damage (wear debris detection on filters) began; it is difficult to judge the failure mechanism from the severely damaged bearing. The second test bearing (the motor side) that did not fail was in the same condition as prior to test.

Dimensional measurements were then made of the DA bearing-machine interfaces and compared to specifications and to the pre-test bearing dimensions to assess whether the bearing-machine fits were correct. Table III shows the major dimensions of the bearings and their relation to installation fits in the DA.

Table III. DA Bearing Overall Fit and Housing Dimensional Measurements, inches

Parameter	Specification	Hub-side bearing	Hub-side bearing fit	Motor-side bearing	Motor-side bearing fit
Outer race outside diameter	3.14960 max 3.14910 min	3.14987	+0.0011 interference	3.14956	+0.0007 interference
Inner race inside diameter	1.9685 max 1.9680 min	1.9681	–0.0007 clearance	1.9681	–0.0005 clearance
Bearing width	0.630 max 0.629 min	0.6296	----	0.6298	----
Radial clearance	0.0014 max 0.0007 min	0.0008	----	0.0008	----

Evaluation of the data in Table III reveals that the failed hub-side bearing's outer diameter was not within specification. Careful measurements were made at two angular locations and at three different width locations. The average is shown in the table. The assembled bearing was under the maximum allowed diameter by approximately 0.0003 in (7.6 µm) at one angular location and over the maximum by 0.0009 in (23 µm) at the other location. The averaged diameter of the hub-side bearing was greater than the maximum allowed by approximately 0.0003 in (7.6 µm). In addition, measurements of the mating DA hub

bore showed that its diameter was undersized by approximately 0.0005 in (13 µm). As installed, this bearing experienced an interference fit with the hub-side housing bore of 0.0011 in (28 µm). This heavy interference fit was outside the design range (0.0001 in (µm)) clearance to 0.0006 in (15 µm) interference) and may be a contributing factor in the bearing failure.

Like the hub-side bearing, the motor-side bearing also had an outside diameter that varied by approximately 0.0006 inch (15 µm) but with an average diameter slightly below the maximum allowed. The motor-side bearing housing diameter was larger than the hub-side bearing housing diameter and was within the specified design range. Taken together, the hub-side bearing, which did fail, was substantially tighter in its DA housing than the motor-side bearing, which did not fail. To evaluate whether these bearing fit differences alone contributed to the failure requires a closer examination of the mating hardware and the stresses and deformation that arise from the installed fits. In particular, it is elucidating to examine any other structural differences between the two bearing locations to determine if other differences such as operating loads exist that could have led to one bearing failing while the other performed well.

Other Differences between Hub and Motor Side Bearing Locations

The hub-side bearing is axially loaded against the motor-side bearing using a calibrated wave spring set to approximately 40 lb (178 N). This is the primary bearing load and results in an average Hertz ball-race contact stress level of approximately 180 Ksi (1240 MPa). In ground testing, the weight of the drum rests on the bearings and can add approximately 20 lb (89 N). In addition, a very small radial load (10 lb (44 N)) is imparted by an O-ring drive belt located slightly outboard of the motor side bearing. Taken together, these loads are considered very low for such a large ball bearing. In effect, both bearings experience similar and low loads that are not likely a contributing factor in the failure.

Aside from the differing levels of interference fits, the most obvious difference between the motor and hub-side bearing locations is the structural design of the housings. As shown in Figures 1 and 5, the motor-side bearing housing has an axial symmetric bowl shape while the hub-side bearing housing is comprised of a shallow cylinder supported by a three-spoke flat plate. The spoke design provides ready physical access to the central portion of the drum to enable the installation of piping and other internal elements. Figure 5(c), for example, shows a close-up view of the hub-side of the drum where a fluid pick-up tube is visible. To determine whether the differences between the hub and motor side housing structures were a contributing factor in the bearing failure, a finite element based analysis was undertaken.

Bearing Installation Fit Considerations - Structural Analysis

The interference (press) fit of a bearing into the bowl-shaped motor-side housing results in the circumferentially uniform compression of the bearing outer race. For steel bearing races, the typical rule of thumb is that the bearing diameter will be reduced by approximately 80% of the fit interference [12]. Since the elastic modulus of NiTi is half that of steel, it is expected that the bearing diameter reduction will be at least this amount, or possibly more. For the motor-side bearing which was known to have an interference level of 0.0007 in (18 µm), we estimate a reduction of about 0.0006 in (15 µm). This level is slightly less than the bearing's internal clearance (0.0008 in (20 µm)) thus leaving an installed clearance of about 0.0002 in (5 µm).

a) Hub side bearing installation

b) motor side bearing installation

Figure 5. End views of DA drum shown during bearing installation. Hub side bearing housing structure (a) differs significantly from motor side (b).

Figure 5(c). Close up end views of hub-side of DA drum showing how the spoke design allows ready access for assembly. Photo taken from [7].

For the hub-side bearing the situation is more nuanced. The known interference fit is larger, 0.0011 in (28 µm). This level of press fit into a circumferentially symmetric and relatively rigid housing would be expected to reduce the bearing diameter by about 0.0009 in (23 µm). This level is greater than the known bearing internal clearance (0.0008 in (20 µm)) resulting in the bearing having no internal clearance and indeed the balls and the inner race would be under a preload by the outer race. This in itself is an undesirable condition that may factor into the hub-side bearing failure. However, the circumferentially non-uniform spoke structure supporting the hub-side bearing housing may cause additional problems in that the installed bearing outer race may not be compressed uniformly.

To estimate the magnitude of the deformations of the hub-side bearing outer race, a finite element model was developed. Figure 6 displays the model result for the axial deformation of the hub-side three-spoke structure under a greater than normal 200-lb (890-N) axial load. The normal axial load for the DA is only 40 lb (178 N). The 200-lb (890-N) case was run to determine whether axial deformation arising from the spring preload could possibly distort the hub-housing geometry. The result was clear. Even under exacerbated axial load the housing shape remains round. It was noted, however, that significant axial deformation of the spokes occurs even under the 40-lb (178-N) design load. This deformation effectively reduces the axial preload through reduction of the distance between the outer races of the hub and

motor-side bearings. Thus if the wave spring height reduction is used to set preload, it is likely that the installed preload will be lower than expected by about 10%.

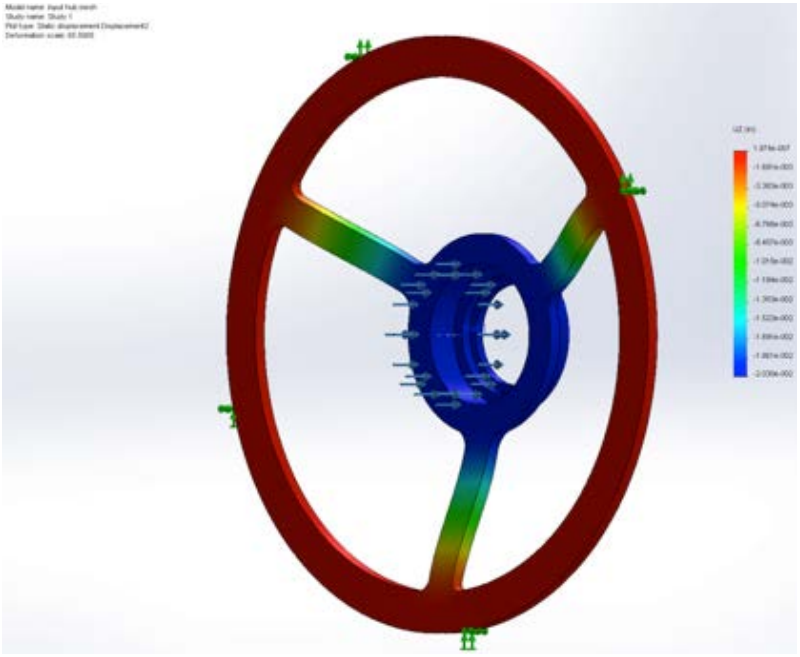

Figure 6. Finite element deformation of the DA hub side structure in response to a large (200-lb (890-N)) axial load. Note that the hub bore remains round

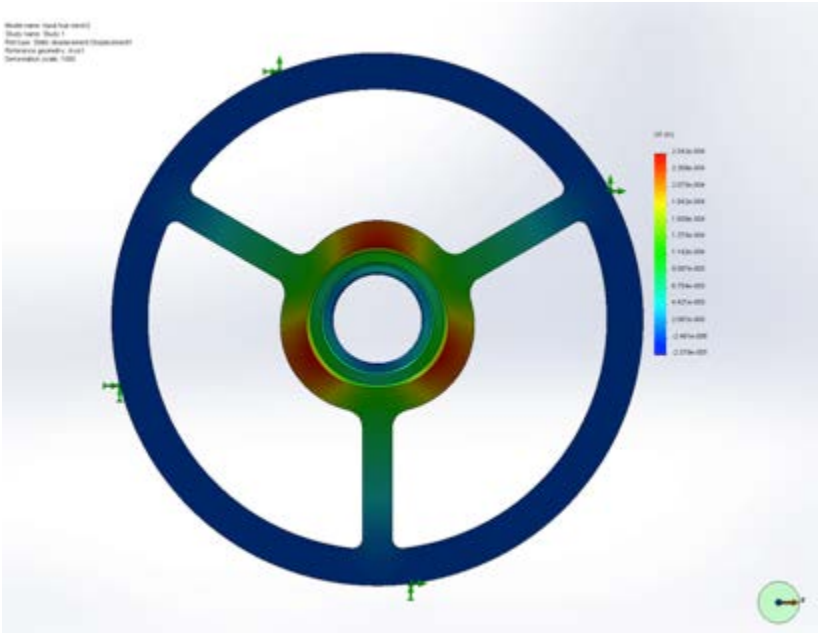

Figure 7. Finite element deformation of the DA hub side structure into which a bearing is installed with a heavy (0.0011 in/28 µm) press fit. Note that the three spoke locations provide high rigidity leading to an irregular bore shape

The second case examined was for a heavy interference press fit (0.0011 in (28 µm) diameter difference) of a round bearing into the circular hub-side housing bore. Figure 7 shows the result.

At the spoke locations, the bearing outer race diameter is reduced by approximately the same magnitude as the bearing clearance and the less rigid housing sections between the spokes allows the bearing housing to take on a tri-lobe shape with radial variation of approximately 0.0002 in (5 µm). Such roundness variation combined with the loss of internal clearance could be responsible for the rapid bearing failure. To corroborate such a root cause theory, however, requires experimental verification.

Bearing Testing-Experimental Corroboration of Failure Theory

The failure of the hub-side bearing in the DA centrifuge after only 200 hr of operation was not anticipated. The operating speed was low (200 rpm) as were the applied external loads. Short-term testing of 60NiTi centrifuge bearings had not surfaced any problems and long-term sub-component 3 ball-on-rod rolling contact fatigue tests suggest infinite life at the design stress levels [13]. However, no long-term life test of a full-scale DA centrifuge bearing had been conducted prior to the failure. Therefore, any bearing tests carried out to corroborate a root cause theory must achieve two goals. First, a bearing test under similar conditions as the failure mode must produce a similar failure in a similar test period. Second, the full-scale, long-term bearing life test under normal design conditions must be done to show that if the factors that contributed to the early failure are ameliorated, long bearing life ensues.

To achieve these two test goals, a series of experiments were conducted in the NASA Glenn DA bearing test rig. This test rig, described in an earlier report on the bearing design and fabrication process, mimics the centrifuge speed, load and other mechanical conditions and can be run continuously and unattended [9]. It does not include the aggressive chemical (wastewater) environment but given 60NiTi's excellent corrosion resistance, the absence of the warm wastewater is not believed to be a failure contributor. The rig is shown in Figure 8.

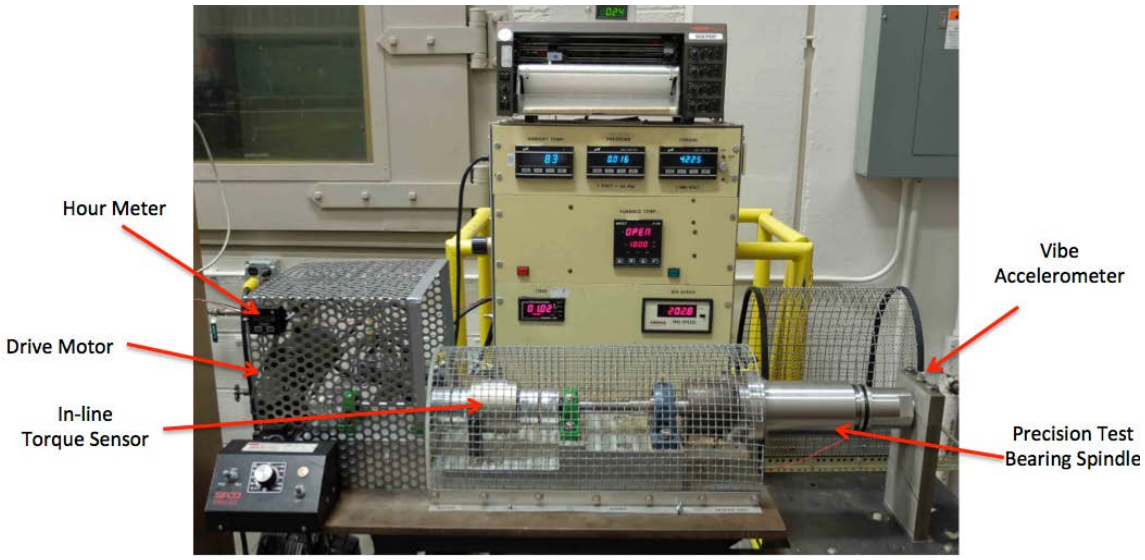

Figure 8. NASA Glenn's DA centrifuge bearing test rig. The present failure corroboration tests are run without water and heat.

Figure 9. Shims used to deform the bearing outer race to match operating conditions in the DA that lead to the premature failure

The first test undertaken was to duplicate the hub-side bearing fit conditions that are believed to have caused the premature bearing failure. This could be achieved by manufacturing a new test rig bearing housing with the same three spoke structure and fit as the DA. Instead, a simplified approach was used that did not require extensive fabrication. The existing cylindrical housing was retained and three small pieces of stainless steel shim stock were placed between the bearing outer race and the housing. These three shims were approximately the same circumferential length and depth as the DA spokes. The shim thickness was selected to deform the bearing outer race approximately the same magnitude as the DA hub side housing. The use of shims is not an exact simulation of the physical race deformations in the DA but it is a fair approximation of the clearance reduction and tri-lobe shape variation. Figure 9 shows a photograph of the bearing outer race and the three shims used for the deformation experiment.

Prior to bearing installation, the shims were affixed to the bearing outside diameter at three equally space locations (120° apart). The bearing housing was warmed to allow a slip fit of the shimmed bearing so as to ensure that the shims were not dislodged. The second test bearing used (simulating the motor-side bearing) was fit normally into the housing with no shims. Despite the shims, the bearings turned smoothly and quietly with low torque. The test began and was monitored for torque once daily.

After 150 hr of test time the bearings continued to turn smoothly. At 157 hr an audible noise was noted and the torque sensor indicated a measurable torque ripple. The test was stopped and the bearings were removed, disassembled and inspected. The shimmed bearing had suffered from fatigue damage. The grease was discolored and wear debris was observed. The fatigue damage resulted in deep raceway pits and spall craters. These were located in the regions that overlapped the shims. The other test bearing that was not shimmed showed no signs of damage. Figure 10 is a close up photograph of the raceway surface of the shimmed outer race after test. Significant surface pitting and spall regions are present. The inner race also showed signs of surface distress (small pits) but it was uniformly distributed around the raceway and less severe.

In the largest spall crater, approximately 4 mm in diameter, cross-race cracks had developed. In some places these cracks had propagated to the outer surface of the race as shown in Figure 11.

Figure 10. Raceway pit developed during shimmed bearing test after 157 hr of run-time

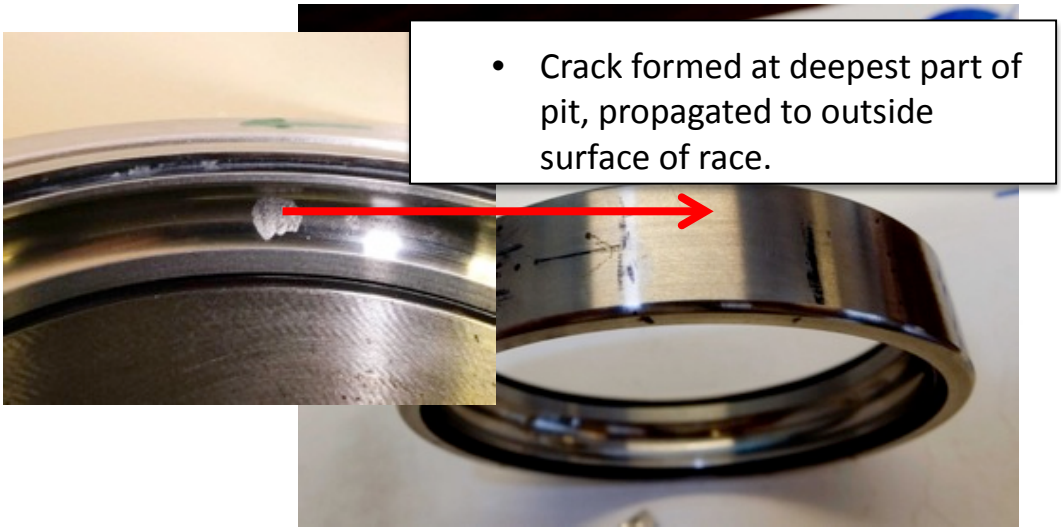

Figure 11. Crack originating in the fatigue spall on raceway has propagated to the outer surface of the race after 157 hr of run-time

If this test been allowed to run longer it is reasonable to expect the damage to progress possibly until the race cracked through completely. Upon reflection, it is possible that the failure path for the DA bearing was surface fatigue followed by pit growth, crack formation and propagation and finally, race fracture. At the onset of the investigation, one theory was that the raceway residual stresses had led to ring fracture and subsequent bearing wear and debris generation. Based upon the shimmed bearing experiment, it appears that ring fracture may have been the final step, not the initiation step.

The second test undertaken was to prove that the 60NiTi bearings have the ability to run for a long-term test without failure, providing they are installed with fits and clearances well accepted as good industry practices. To conduct this test, a pair of flight quality 60NiTi bearings was carefully inspected, cleaned and lubricated. The pair was then installed into the NASA Glenn test rig with fits within the specified design range. The inner races had a clearance (shaft to bearing diameter) of 0.0005 in (13 µm) and the outer races had a slight interference fit of 0.0003 in (7.6 µm). In our test rig, the outer race housing does not have spokes, thus any outer race deformation is circumferentially symmetric.

In addition, an accelerometer was installed on the stationary inner shaft to monitor the rig vibration. Once each hour the full frequency range (sub-hertz to 100 Hz) is collected and stored. Comparison of these spectra over the course of the test allow for careful health monitoring. Any vibration growth at relevant frequencies (e.g., at the run speed, ball pass frequencies, cage frequency) would be cause for bearing inspection. Figure 12 shows a representative cascade plot of hourly vibration spectra collected over a three-day test period.

The cascade vibration plot provides a convenient visual method to judge bearing condition. Each peak in the spectra corresponds to different aspects of the test rig and test bearing. For example, vibration at the rig speed (3.2 Hz or 200 rpm) would arise from any anomaly associated with the drive motor, couplings or drive shafts. Vibrations generated by the test rig support bearings arise at 22 Hz owing to the number of rolling elements and internal geometry of these bearings. The test rig structure has some activity at 37 Hz. A key test bearing frequency for health monitoring is 24 Hz. This frequency represents the ball pass frequency on the inner race. Slight roundness and other variations will lead to vibration at this frequency. Any significant increase in the amplitude at 24 Hz could signal raceway surface damage in the ball path. Thus the cascade plot serves as a snapshot of bearing health.

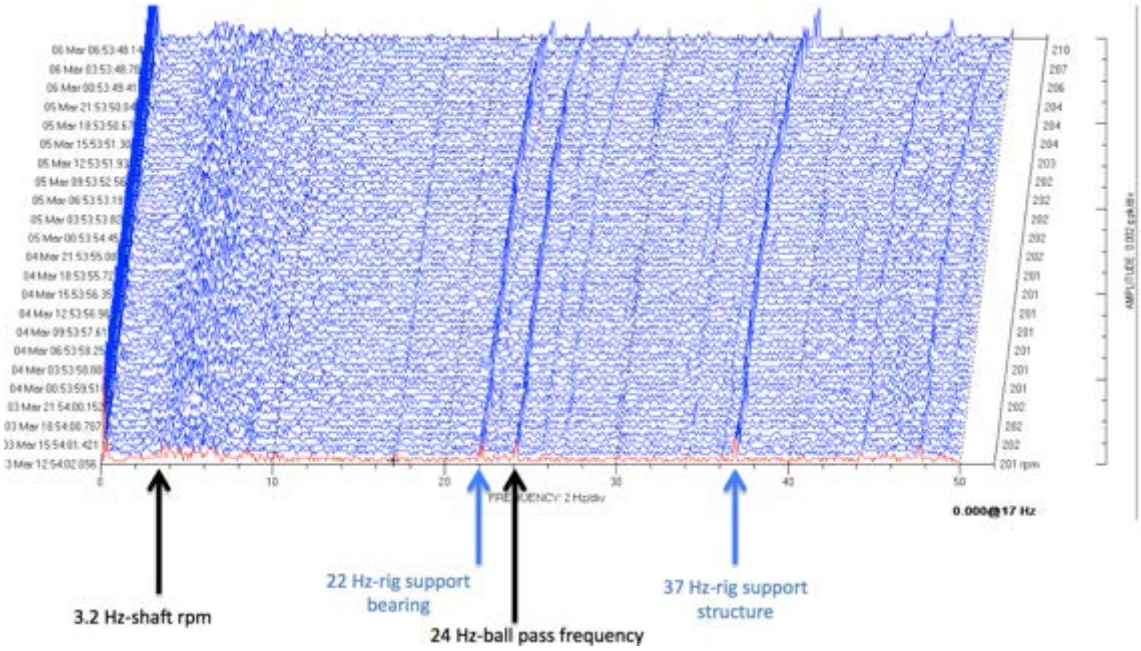

Figure 12. Cascade plot of hourly test rig vibration spectra captured during a three-day test period. Overall vibrations are very low and consistent

Prior to the start of this second test, the bearings were disassembled, solvent cleaned, visually inspected, reassembled and greased (30% fill of the free-volume) with a lithium complex synthetic grease. The bearings were then installed into the test rig and the preload spring was adjusted to 90-lb (400-N) preload to match the preload level generally recommended by bearing manufacturers for this size bearing [12]. This preload is higher than the application design preload (40 lb / 178 N) but that lower load level was selected based upon the more modest static load capability of the prior bearing material made from a softer cobalt alloy [9]. Further, the higher load level may offer an acceleration of any fatigue failure modes. Thus, if the bearings indeed survive the life test, the root cause theory and recovery path is better substantiated.

The life test was begun and vibration data collected. At first there was a noticeable torque ripple measured. After a few hours of run time the torque ripple subsided and the cascade plot stabilized

probably because the grease had become more uniformly distributed in the bearing. The life-test period is 5000 hr. Once during test period (1075 hr) a bearing inspection was conducted. Figure 13 shows images of one of the bearings during the interim inspection.

During the inspection the races were examined under 10x optical magnification and appeared to be in excellent condition. They exhibited no surface pits, scratches or wear tracks. Also, the retainer was unworn and the grease color and consistency was the same as the beginning-of-test. Following the inspection, the bearings were solvent cleaned, re-greased and installed back into the test rig. After a few hours of operation the torque ripple subsided leaving a vibration spectra that resembled one from before the inspection.

Figure 13. Photograph of the test bearing during an interim inspection at 1075 hr. Overall condition of the bearing races, balls and retainer was unchanged from beginning of test. The grease consistency and color was also unchanged

The life-test concluded at 5000 hr because it met the project requirement. More important, the successful life test helps to corroborate the root cause theory by showing that a set of bearings, when properly fit into the machine structure can operate without failure for long periods.

Root Cause Failure Theory and Recovery Plan

The forensic examination of the failed bearing, subsequent measurements of the related machine hardware, and corroborative bearing tests supports the root cause theory that an overly tight interference press fit and a non-symmetric housing structure led to surface fatigue damage to the 60NiTi bearing. The

surface damage then progressed until the inner race cracked through its thickness and the operation was suspended. To avoid this failure mode the following remediation steps are indicated.

Selective fitting of the bearings, especially in the hub-side DA housing, should be done to seek a fit in which the bearing outside diameter and the hub bore diameter are as closely matched as possible. The design calls for a range of 0.0001 in (2.5 µm) clearance to 0.0006 in (15 µm) interference. Another approach is to manufacture bearings with varying diameters to accommodate future DA machines with less or no interference thus avoiding the deleterious effects of outer race distortion and loss of internal clearance. Furthermore, bearings with larger internal clearances can be used so that any outer race press fit will not result in a significant or even complete loss of internal ball-to-race clearance. Conversely, bearing designs less sensitive to internal clearance variations, such as angular contact bearings, could be considered.

Concluding Remarks

NiTi bearing technology is still relatively immature. Therefore, when problems such as this unexpected bearing failure arise, it is natural to infer that the new material is a cause. Indeed in this case, the low elastic modulus of 60NiTi compared to steel results in more pronounced race deformation due to hub bore interface effects like shape and diameter interference. It is possible that a similarly dimensioned steel bearing would not have failed because the outer race deformations would have been smaller.

For these reasons, it is essential that extra care be taken when using 60NiTi bearings to ensure that all industry accepted engineering and application practices are followed. Going forward, it is likely that the experience base for the use of these materials will grow and this will support the emergence of new best practices. By adopting these practices, the mechanisms community will be able to capitalize on NiTi's excellent corrosion resistance and static load capability properties.

Acknowledgments

The authors wish to thank Anita Howard, Walt Schneider and Mike Perry of the NASA Marshall Space Flight Center for their thoughtful technical input. We thank Walt Wozniak and Steve Miller at the NASA Glenn Research Center for their technical efforts to build the test hardware to corroborate the root cause theory. Finally, we thank NASA Glenn's Penni Dalton for her steadfast project management support and for standing behind our progress despite setbacks and other challenges. We have benefitted from the perseverance and dedication of these colleagues.

References

1. W.J. Derner and E.E. Pfaffenberger: “Rolling Element Bearings,” in CRC Handbook of Lubrication, volume II, pages 495-537, edited by E.R. Booser, CRC Press, Boca Raton, 1983.
2. J.L. Radovich: “Gears”, in CRC Handbook of Lubrication, volume II, pages 539-564, edited by E.R. Booser, CRC Press, Boca Raton, 1983.
3. C. DellaCorte: “Novel Superelastic Materials for Advanced Bearing Applications”, Presented at 13th International Ceramics Conference of CIMTECH 2014, Montecatini, Italy, June 8-13. Published in Advances in Science and Technology, volume 89 (2014), pp 1-9, 2014.
4. C. DellaCorte, S. V. Pepper, R. D. Noebe, D.R. Hull, and G. Glennon: “Intermetallic Nickel-Titanium Alloys for Oil-Lubrication Bearing Applications,” NASA TM-2009-215646, March 2009.
5. S. V. Pepper, C. DellaCorte, R. D. Noebe, D.R. Hull, and G. Glennon: “Nitinol 60 as a Material for Spacecraft Triboelements,” ESMATS 13 Conference, Vienna, Austria, September 2009.
6. C. DellaCorte, R.D. Noebe, M.K. Stanford, and S.A. Padula: “Resilient and Corrosion-Proof Rolling Element Bearings Made From Superelastic Ni-Ti Alloys for Aerospace Mechanism Applications,” NASA TM-2011-217105, September 2012.
7. D.L. Carter: “Status of the Rengenerative ECLSS Water Recovery System”, Paper number M10-0762, AIAA International Conference on Environmental Systems; 11-16 July, Barcelona, Spain, 2010.
8. D.W. Holder and C.F. Hutchens: “Development Status of the International Space Station Urine Processor Assembly,” SAE 2003-01-2690, 33rd International Conference on Environmental Systems, July 7-10, Vancouver British Columbia, 2003.
9. C. DellaCorte, and W.A. Wozniak: “Design and Manufacturing Considerations for Shockproof and Corrosion-Immune Superelastic Nickel-Titanium Bearings for a Space Station Application”, NASA TM 2012-216015, presented at the 41st Aerospace Mechanisms Symposium, Pasadena, CA, May 2012.
10. M.K. Stanford, F. Thomas, and C. DellaCorte: “Processing Issues for Preliminary Melts of the Intermetallic Compound 60-NITINOL,” NASA TM-2012-216044, November 2012.
11. M.K. Stanford, W.A. Wozniak, and T.R. McCue: “Addressing Machining Issues for the Intermetallic Compound 60-NITINOL,” NASA TM-2012-216027, August 2012.
12. Barden Super Precision Ball Bearings Catalogue, D/SPC/1/USA/113/T, Danbury, CT, 2013.
13. C. DellaCorte, M.K. Stanford, and T.R. Jett: “Rolling Contact Fatigue of Superelastic Intermetallic Materials (SIM) for Use as Resilient and Corrosion Resistant Bearings,” Tribology Letters, (2015) 57:26, January 23rd, 2015.